Geosci. Model Dev. Discuss., doi:10.5194/gmd-2016-300, 2017
Manuscript under review for journal Geosci. Model Dev.
Published: 10 January 2017

Geoscientific Model Development Discussions

The Analytical Objective Hysteresis Model (AnOHM v1.0): Methodology to Determine Bulk Storage Heat Flux Coefficients

Ting Sun[1,2,3*], Zhi-Hua Wang[4], Walter C. Oechel[5,6], Sue Grimmond[1*]

[1]Department of Meteorology, University of Reading, Reading RG6 6BB, UK
[2]Department of Hydraulic Engineering, Tsinghua University, Beijing 100084, China
[3]State Key Laboratory of Hydro-Science and Engineering, Tsinghua University, Beijing 100084, China
[4]School of Sustainable Engineering and the Built Environment, Arizona State University, Tempe, AZ 85287, US
[5]Global Change Research Group, Department of Biology, San Diego State University, San Diego, CA 92182, US
[6]Department of Environment, Earth and Ecosystems, The Open University, Milton Keynes MK7 6AA, UK

Correspondence to: Ting Sun (ting.sun@reading.ac.uk); Sue Grimmond (c.s.grimmond@reading.ac.uk)

Abstract. The net storage heat flux is not only a large part of the urban surface energy balance (SEB) but its determination remains a significant challenge. The diurnal hysteresis behaviour found between the net storage heat flux (ΔQ_S) and net all-wave radiation (Q^*) has been captured in the Objective Hysteresis Model (OHM) parametrization of ΔQ_S. Although, successfully used in urban areas, the limited availability of coefficients for OHM hampers application. To facilitate use, and enhance physical interpretations of the OHM coefficients, an analytical solution of the 1-dimensional advection-diffusion equation of coupled heat and liquid water transport in conjunction with the SEB is conducted, allowing development of AnOHM (Analytical Objective Hysteresis Model). A sensitivity test of AnOHM to surface properties and hydrometeorological forcing is undertaken using a stochastic approach (the Subset Simulation). From this albedo, Bowen ratio and bulk transfer coefficient, solar radiation and wind speed are identified as being critical. AnOHM, driven by local meteorological conditions at five different land use areas, is shown to simulate the ΔQ_S flux well (RMSE values of ~30 W m^{-2}). The intra-annual dynamics of OHM coefficients to are explored which offers significant potential to enhance modelling of the surface energy balance over a wider range of conditions.

1 Introduction

The essential role of an integrated land surface model is to physically predict the land-atmosphere interactions by resolving the transfer of energy, water, and trace gases (Katul et al., 2012; Liang et al., 1994; Sellers et al., 1997). Such land-atmospheric interactions are strongly modulated by the solar energy partitioning at the land surface (Chen and Dudhia, 2001; McCumber and Pielke, 1981; Yang and Wang, 2014). The surface energy balance (SEB) equation is (Oke, 1988):

$$Q^* - \Delta Q_S = Q_H + Q_E \tag{1}$$

where Q^*, ΔQ_S, Q_H and Q_E are the net all-wave radiation, net storage, turbulent sensible and latent heat fluxes, respectively. Eqn (1) distinguishes the available energy at the land surface (left hand side) from the heat transfer through turbulent transport (right hand side).

The turbulent and radiative fluxes are more readily measured using standard techniques (e.g., eddy-covariance instruments, radiometry, etc.), than ΔQ_S because of spatially sampling associated with the instrumental techniques (Offerle et al., 2005; Pauwels and Daly, 2016; Roberts et al., 2006; Wang, 2012). This is because the net energy stored or released by changes in sensible heat within the canopy air layer, roughness elements (RE, e.g. vegetation, buildings) and the ground have to be considered. The volume of interest extends from the top of the roughness sub-layer to the depth in the ground where the vertical net heat conduction is zero on a daily basis (see Figure 2 in Masson et al., 2002).

Knowledge of ΔQ_S is crucial to a wide range of processes and applications: from modelling turbulent heat transfer and boundary layer development to predicting soil thermal fields*, etc*.. In rural or simple bare soil sites, this term may be a small fraction of the net all wave radiation (e.g. 5%) but in areas where there is more mass, such as cities, the term becomes much more significant. In urban areas, the large amount of mass made from high heat-admitting materials is arranged in canyon morphology. These features are critical in causing the urban heat island, through radiative trapping and the thermal inertia due to this storage term.

Practical difficulties of direct measurement of ΔQ_S in urban areas, result in the SEB residual (i.e., $Q^* + Q_F - (Q_H + Q_E)$) frequently being the "best" observations (Ao et al., 2016; Li et al., 2015), where Q_F is the anthropogenic heat flux. A wide range of techniques are used to obtain ΔQ_S in urban systems (Grimmond et al., 1991; Roberts et al., 2009). These include:

a) Heat conduction approach: the weighted average of heat flows through all urban materials and surfaces by solving heat conduction equation (e.g., buildings, streets, vegetated lands, etc.) (Offerle et al., 2005; Wang et al., 2012; Yang et al., 2014);
b) Residual approach: the urban SEB residual given other terms modelled or measured (Ching et al., 1983; Doll et al., 1985; Oke and Cleugh, 1987);
c) Thermal mass scheme: the storage heat is inferred from the changes in thermal mass of all components of the urban system (Kerschgens and Kraus, 1990).
d) Composite of heat flux plates: Kerschgens and Hacker (1985) and Kerschgens and Draushke (1986) combined measurements from grass and paved surfaces;
e) Parameterisation of Q^*: linear function of Q^* (Oke et al., 1981); hyperbolic (*cotangent*, *secant*) function (Doll et al., 1985); and hysteresis relation between ΔQ_S and Q^* (Camuffo and Bernardi, 1982) used in the Objective Hysteresis Model (OHM) (Grimmond et al., 1991)

Geosci. Model Dev. Discuss., doi:10.5194/gmd-2016-300, 2017
Manuscript under review for journal Geosci. Model Dev.
Published: 10 January 2017

Geoscientific Model Development Discussions
Open Access

The focus here is on the OHM approach, which is forced by Q^* and accounts for the diversity of the surface by 2 or 3-dimensional weighting (*f*) of the sub-facets (*i*) materials (Grimmond et al., 1991):

$$\Delta Q_S = \sum_i f_i \left(a_{1,i} Q_i^* + a_{2,i} \frac{\partial Q_i^*}{\partial t} + a_{3,i} \right) \quad (2)$$

where the a_1, a_2 and a_3 coefficients are for individual facets determined by observation (e.g. asphalt road (Anandakumar, 1999), wetland (Souch et al., 1998), forests (Oliphant et al., 2004)) or numerical modelling (e.g. urban canyons (Arnfield and Grimmond, 1998), roofs (Meyn and Oke, 2009)). The coefficients provide a net behaviour of a facet type in a typical setting, rather than being required to identify the component materials within a facet (e.g. multiple materials making up a roof, wall, with varying thermal connectivity and individual properties).

Despite the shortage of OHM coefficients for the wide range facet types, OHM captures the urban SEB processes (Grimmond and Oke, 1999; Järvi et al., 2011; 2014; Karsisto et al., 2015; Roth and Oke, 1995). OHM is a cornerstone in the urban land surface models, Surface Urban Energy and Water Balance Scheme (SUEWS) (Järvi et al., 2011; 2014; Ward et al., 2016) and Local-scale Urban Meteorological Parameterisation Scheme (LUMPS) (Grimmond and Oke, 2002), and plays an essential role in determining the initial energy partitioning at each time step of the models' simulations. Previous modelling studies (Arnfield and Grimmond, 1998; Meyn and Oke, 2009) have led to better understanding of the OHM coefficients. Although, Gao et al. (2003; 2008) solved the 1-dimensional advection-diffusion equation of coupled heat and liquid water transport to explore the physical relation of OHM coefficients a_1 and a_2 to the phase lag between ΔQ_S and Q^*, insight into a_3 remains unclear (Sun et al., 2013).

In this paper, the solutions of the one-dimensional advection-diffusion equation of coupled heat and liquid water transport (Gao et al., 2003; 2008) are employed with the SEB (eqn 1) to investigate more fully the three OHM coefficients to allow development of the Analytical Objective Hysteresis Model (AnOHM) (section 2). Sensitivity analysis of AnOHM to surface properties and hydrometeorological conditions is undertaken using Monte Carlo-based Subset Simulation (Au and Beck, 2001) (section 3). An offline evaluation of AnOHM's performance for five sites with different land covers (section 4) allows us to conclude that this is an alternative approach to obtain OHM coefficients. As this will allow application across a much wider range of environments and meteorological conditions, it has important implications for land surface modelling (urban and non-urban).

Geosci. Model Dev. Discuss., doi:10.5194/gmd-2016-300, 2017
Manuscript under review for journal Geosci. Model Dev.
Published: 10 January 2017

Geoscientific Model Development Discussions
Open Access

2 Model Development

2.1 Parameterization of Storage Heat Flux ΔQ_S for a Land Surface

For a given land surface (e.g. bare soil), the governing heat conduction-advection equation can be written (Gao et al., 2003; 2010):

$$\frac{\partial T}{\partial t} = \lambda \frac{\partial^2 T}{dz^2} + W \frac{\partial T}{\partial z} \tag{3}$$

where T is the temperature at a reference depth z (positive downward), λ is the thermal diffusivity and $W = \partial\lambda/\partial z - (C_W/C_g)w\varphi$ is the soil water flux density (Ren et al., 2000), with C_W the volumetric heat capacity of water, C_g the volumetric heat capacity of soil, w the pore water velocity, and φ the volumetric soil water content.

The steady-periodic solution of equation (3), corresponding to the principle Earth's rotation frequency ($\omega = 2\pi/24$, in rad h^{-1}), is given by:

$$T(z,t) = A_{T_S} \exp(-z/M) \sin(\omega t - z/N - \gamma) + \overline{T_S} \tag{4}$$

where $M = \frac{2\lambda}{\Delta + W}$, $N = \frac{\Delta}{\omega}$ and $\Delta = \sqrt{\frac{W^2+\sqrt{W^4+16\lambda^2\omega^2}}{2}}$; and $\overline{T_S}$, A_{T_S} and γ denote the daily mean value, amplitude and initial phase of surface temperature, respectively, which need to be determined by the boundary conditions imposed by the SEB.

From Fourier's law, the soil heat flux is then given by:

$$G(z,t) \equiv -\frac{k\partial T}{\partial z} = kA_{T_S}\frac{\sqrt{M^2+N^2}}{MN} \exp\left(-\frac{z}{M}\right) \sin\left(\omega t - \frac{z}{N} - \gamma + \delta\right) \tag{5}$$

where $\delta = \arctan\left(\frac{M}{N}\right) = \arctan\left[\frac{2\lambda\omega}{(\Delta+W)\Delta}\right]$ and k is the thermal conductivity. In particular, at the surface $z = 0$, the ground heat flux G_0 and surface temperature T_s are given by:

$$G_0(t) = kA_{T_S}\frac{\sqrt{M^2+N^2}}{M\,N}\sin(\omega t - \gamma + \delta), \tag{6}$$

$$T_S = A_{T_S}\sin(\omega t - \gamma) + \overline{T_S} \tag{7}$$

And a simple written form of ΔQ_S (if only one surface) can be given as:

$$\Delta Q_S = G_0 = c_\eta \sin(\omega t + \eta) \tag{8}$$

where $\eta = \delta - \gamma$ and $c_\eta = kA_{T_S}\frac{\sqrt{M^2+N^2}}{MN}$.

It is noted although the above derivation only considers the land surface made of single material type, the derived ΔQ_S (eqn 8) can be adapted for surfaces made of composite materials or volumes given appropriate bulk/ensemble properties.

Geosci. Model Dev. Discuss., doi:10.5194/gmd-2016-300, 2017
Manuscript under review for journal Geosci. Model Dev.
Published: 10 January 2017

2.2 Parameterization of Net All-wave Radiation Q^* for a Land Surface

Given the parameterizations of incoming longwave radiation $L_{\downarrow}$, outgoing longwave radiation $L_{\uparrow}$, sensible heat flux Q_H, latent heat flux Q_E, and storage heat flux ΔQ_S as follows:

$$L_{\downarrow} = \varepsilon_a \sigma T_a^4, \quad (9)$$

$$L_{\uparrow} = \varepsilon_s \sigma T_S^4, \quad (10)$$

$$Q_H = C_h U (T_S - T_a), \quad (11)$$

$$Q_E = Q_H / \beta, \quad (12)$$

$$\Delta Q_S = G_0, \quad (13)$$

the boundary condition imposed by the SEB relation can be rewritten as:

$$(1-\alpha) K_{\downarrow} + \varepsilon_a \sigma T_a^4 - \varepsilon_s \sigma T_S^4 = C_h U (1 + \beta^{-1})(T_S - T_a) + G_0 \quad (14)$$

where the turbulent fluxes Q_H and Q_E are parameterized as functions of temperature gradient $T_S - T_a$ with bulk transfer coefficient C_h, wind speed U and Bowen ratio (β=Q_H/Q_E).

By assuming the incoming solar radiation $K_{\downarrow}$ and air temperature T_a follow sinusoidal forms through a day as function of the mean value for the day (e.g. $\overline{K_{\downarrow}}$):

$$K_{\downarrow} = A_K \sin(\omega t) + \overline{K_{\downarrow}} \quad (15)$$

$$T_a = A_T \sin(\omega t - \tau) + \overline{T_a} \quad (16)$$

and introducing the solar radiation scale:

$$A_K^* = (1-\alpha) A_K \quad (17)$$

and longwave radiation scale (assuming $\varepsilon_a \approx \varepsilon_s \approx \varepsilon$ as a first order; cf. clear sky of ~0.85 (Staley and Jurica, 1972) and urban surfaces of ~0.95 (Kotthaus et al., 2014)):

$$A_T^* = \left(4\varepsilon\sigma\overline{T_a}^3 + (1+\beta^{-1}) C_h U\right) A_T = (f_L + f_T) A_T = f A_T \quad (18)$$

where τ denotes phase difference between T_a and $K_{\downarrow}$, the $f = f_L + f_T$ consists of the longwave energy redistribution factor: $f_L = 4\varepsilon\sigma\overline{T_a}^3$ and a turbulent energy redistribution factor: $f_T = (1+\beta^{-1}) C_h U$. Linearizing the fourth-order longwave expressions of temperature at mean daily air temperature $\overline{T_a}$ (Sun et al., 2013), the values of $\overline{T_S}$ and A_{T_S} are obtained:

Geosci. Model Dev. Discuss., doi:10.5194/gmd-2016-300, 2017
Manuscript under review for journal Geosci. Model Dev.
Published: 10 January 2017

Geoscientific Model Development Discussions Open Access

$$\overline{T_S} = \frac{1-\alpha}{f}\overline{K_\downarrow} + \overline{T_a} \tag{19}$$

$$\begin{aligned} A_{T_S} &= \frac{fMN\sin(\tau)}{N(fM+k)\sin(\gamma) - kM\cos(\gamma)}A_T \\ &= \frac{1}{\sqrt{M_*^2+N_*^2}}\frac{\sin(\tau)}{\sin(\gamma-\zeta)}A_T \\ &= \chi_\gamma A_T \end{aligned} \tag{20}$$

where $\zeta = \arctan(N_*/M_*)$, $\gamma = \zeta + \arctan\left(\frac{\sin(\tau)}{\cos(\tau)+A_K^*/A_T^*}\right)$, $M_* = 1 + k/(fM)$, $N_* = k/(fN)$ and $\chi_\gamma = \frac{1}{\sqrt{M_*^2+N_*^2}}\frac{\sin(\tau)}{\sin(\gamma-\zeta)}$.

The net all-wave radiation Q^* is parameterized as:

$$\begin{aligned} Q^* &= (1-\alpha)K_\downarrow + 4\varepsilon\sigma T_a^4 - 4\varepsilon\sigma T_S^4 \\ &= (1-\alpha)\left(A_K\sin(\omega t) + \overline{K_\downarrow}\right) + f_L(T_a - T_S) \\ &= c_\varphi\sin(\omega t+\varphi) + \frac{f_L}{f}(1-\alpha)\overline{K_\downarrow} \end{aligned} \tag{21}$$

where $\varphi = \arctan\left[\frac{(\chi_\gamma\sin(\gamma)-\sin(\tau))}{(fA_K^*)/(f_LA_T^*)-(\chi_\gamma\cos(\gamma)-\cos(\tau))}\right]$ and $c_\varphi = \sqrt{\left[\frac{(fA_K^*)^2}{(f_LA_T^*)^2} - (\chi_\gamma\cos(\gamma)-\cos(\tau))\right]^2 + [\beta_\gamma\sin(\gamma)-\sin(\tau)]^2}$.

2.3 Derivation of AnOHM coefficients

Based on the above parameterizations of Q^* and ΔQ_S, together with OHM for a specific surface:

$$\Delta Q_S = a_1 Q^* + a_2\frac{\partial Q^*}{\partial t} + a_3, \tag{22}$$

the coefficients can be readily derived from the parameterization in section 2.2, as:

$$a_1 = \frac{c_\eta}{c_\varphi}\cos(\eta-\varphi) \tag{23}$$

$$a_2 = \frac{c_\eta}{\omega c_\varphi}\sin(\eta-\varphi) \tag{24}$$

$$\begin{aligned} a_3 &= -\frac{c_\eta}{c_\varphi}\cos(\eta-\varphi)\cdot\frac{f_T}{f}(1-\alpha)\overline{K_\downarrow} \\ &= -a_1\cdot\frac{f_T}{f}(1-\alpha)\overline{K_\downarrow} \end{aligned} \tag{25}$$

Geosci. Model Dev. Discuss., doi:10.5194/gmd-2016-300, 2017
Manuscript under review for journal Geosci. Model Dev.
Published: 10 January 2017

Geoscientific Model Development
Discussions
Open Access

In the densest parts of cities, the anthropogenic heat (Q_F) often has a large influence on the SEB that needs to be accounted for (Allen et al., 2011; Chow et al., 2014; Nie et al., 2014; Sailor, 2011). This requires the governing SEB relation (eqn 14) to be rewritten:

$$(1-\alpha)K_\downarrow + \varepsilon\sigma T_a^4 - \varepsilon\sigma T_S^4 + Q_F = C_h U(1+\beta^{-1})(T_S - T_a) + G_0 \tag{26}$$

Assuming Q_F is diurnally invariant (as a first order estimate e.g. Best and Grimmond (2016)), the derivation (section 2.2) can be extended to include a first order estimate of Q_F to obtain:

$$\begin{aligned} a_{3F} &= -\frac{c_\eta}{c_\varphi}\cos(\eta-\varphi)\cdot\frac{f_T}{f}(1-\alpha)\overline{K_\downarrow} - Q_F \\ &= -a_1\cdot\frac{f_T}{f}(1-\alpha)\overline{K_\downarrow} - Q_F \end{aligned} \tag{27}$$

where a_{3F} (subscript 'F' indicates the inclusion of Q_F). The other two coefficients remain unchanged.

2.4 Physical Interpretations of AnOHM Coefficients

Based on the parameterizations of AnOHM coefficients (eqns 23, 24, 25/27), the physical interpretations are as follows:

a) a_1 characterizes the ratio of ΔQ_S and Q^* and depends on the energy scales (i.e. c_η and c_φ) and their phase difference (i.e. $\eta-\varphi$);

b) a_2 accounts for the temporal changes in ΔQ_S and Q^* by including the principle Earth's rotation frequency ω, in addition to the same determinants of a_1 (i.e. c_η, c_φ and $\eta-\varphi$);

c) a_3 (or a_{3F}) indicates the baseline ΔQ_S determined by energy redistribution factors (i.e. f_T and f) and energy inputs (i.e. $\overline{K_\downarrow}$, and Q_F if anthropogenic heat is considered) as well as a_1.

3 Sensitivity Analysis

Due to the complex dependence of AnOHM coefficients on surface properties and meteorological forcing (section 2.3), the impacts of these coefficients are further assessed by a sensitivity analysis.

Geosci. Model Dev. Discuss., doi:10.5194/gmd-2016-300, 2017
Manuscript under review for journal Geosci. Model Dev.
Published: 10 January 2017

Geoscientific Model Development Discussions

3.1 Subset Simulation

To improve the computational efficiency of undertaking Monte Carlo sensitivity analyses, subset simulation is used (Au and Beck, 2001). This is an adaptive stochastic simulation procedure with particular efficiency in analysing the short-tail of a distribution probability (while also adaptable to long-tail scenarios) (Wang et al., 2011).

If the probability that a critical response Y exceeds a threshold y, $P(Y > y)$, a range of exceedance regions can be specified and sampled using Markov chains. Initially a direct Monte Carlo method is used to choose possible values for the parameter of interest in the anticipated range with a specified distribution (or probability distribution function, PDF) of the uncertainty. From this (level 0), the first exceedance level probability is determined, F_1 at which $P(Y > y_1)$. Then a Markov chain Monte Carlo (MCMC) procedure is used to generate samples of a given conditional probability p_0, leading to the exceedance of y_1 in the earlier simulations. This procedure is repeated, for exceedance events F_i at which $P(Y > y_i) = p_0^i$, $i = 1, 2, 3, \ldots$, until simulations reach a target exceedance probability, e.g. associated with rare events or risk analysis. Further details of this subset simulation process are provided in Wang et al. (2011).

Subset simulation efficiently generates conditional samples with Metropolis algorithms (Hastings, 1970; Metropolis et al., 1953). This is the basis of MCMC. To generate samples that successively approach a certain conditional probability, a specific Markov chain is designed with the target PDF as its limiting stationary distribution trend as its length increases. The selection of proposal distributions is the key as this controls the next sample generated based on the current one. Ideally, the distribution selection would be automatic but this has an efficiency cost relative to the robustness benefit. For the surface parameters (Table 1a) and hydrometeorological forcing (Table 1b) analyses (Stull, 1988) a normal distribution PDF is used (Au and Beck, 2003; Au et al., 2007), with three conditional levels (N_{level}=3) and a conditional probability of $p_0 = 0.1$: i.e., at each level the highest 10% of the outputs are considered to exceed the intermediate threshold. As such, the three-level simulation can effectively capture a rare event with the target exceedance probability of 10^{-4} (i.e., the probability of occurrence is less than 1 in 10000) and generate appropriate samples of different conditional probabilities.

The metric S (in %), used to indicate the sensitivity of the model output Y to a specific uncertainty parameter X (Wang et al., 2011), is:

$$\mathrm{S} = \left[\frac{1}{N_{\text{level}}}\sum_{i=1}^{N_{\text{level}}}\frac{E[X|Y > y_i] - E[X]}{E[X]}\right]\times 100 \quad (28)$$

where $i = 1, 2, \ldots, N_{\text{level}}$ is the index of conditional sampling level, $E[X]$ is the expectation that the unconditional distribution of a specific uncertainty parameter X, while $E[X|Y > y_i]$ is the expectation of X at conditional level i. A positive (negative) S

Geosci. Model Dev. Discuss., doi:10.5194/gmd-2016-300, 2017
Manuscript under review for journal Geosci. Model Dev.
Published: 10 January 2017

indicates an increase will lead to increase (decrease) in simulated value, hence the sign of S indicates the impact of a change in parameter uncertainty. The absolute magnitude of S indicates the sensitivity.

This assessment does not consider if the simulated values have low probability. Later analyses (section 4) consider the simulation results relative to observed fluxes.

3.2 Impacts of Surface Properties

Following the sensitivity analysis of AnOHM coefficients to the surface properties, the distributions of conditional samples for thermal conductivity k, bulk heat capacity C_p and emissivity ε are similar to the original proposal distributions (Figure 1), implying weak dependence of a_1, a_2 and a_3 on these properties. However, for albedo (α) both a_2 and a_3 are sensitive but a_1 is not; changes in inverse Bowen ratio (β^{-1}) impact all three coefficients; and bulk transfer coefficient C_h impacts a_1 and a_2, but has little effect for a_3.

Using S (eqn 28) to quantify this, it is found that the surface properties (k, C_p and ε) have less sensitivity, with less skewed conditional samples between levels, so S values close to 0 (Figure 2). The S of k is the largest of the three. From the S results for the α sensitivity analysis (Figure 2), it is apparent that an increase in α will increase a_1 while decreasing a_2 and a_3, whereas the reverse occurs for β^{-1} and C_h – i.e. their decreases leads to larger a_2 and a_3 values but smaller a_1.

From this, the links between the key surface parameters and the storage heat flux can be considered. With an increase in α, there is reduced solar energy in the SEB - this reduces the temporal change in ΔQ_S (smaller a_2) and decreases the baseline value of ΔQ_S (smaller a_3); larger β^{-1} indicates more available energy is dissipated by Q_E than by Q_H, leading to decreased T_s and ΔQ_S (smaller a_1); a smaller portion of Q^* will be dissipated by ΔQ_S (smaller a_1) as the increased C_h can facilitate the turbulent convection and thus increase the total turbulent fluxes.

3.3 Impacts of Hydrometeorological Conditions

Similarly, the sensitivity of AnOHM to hydrometeorological variables is explored (Figure 3). The air temperature (range, mean) and water flux density related variables (i.e. A_T, $\overline{T_a}$ and W) have minimal influence on the skewness of the conditional samples. In contrast, the incoming shortwave (solar) radiation (range, mean) and wind related variables (i.e. A_K, $\overline{K_\downarrow}$ and U) and the phase lag τ between $K_\downarrow$ and T_a have large impacts. In terms of the greatest impact on the coefficients (a_1, a_2 and a_3): A_K and U influences a_1, τ impacts a_2, and a_3 responds more to A_K and $\overline{K_\downarrow}$ than the other variables.

Geosci. Model Dev. Discuss., doi:10.5194/gmd-2016-300, 2017
Manuscript under review for journal Geosci. Model Dev.
Published: 10 January 2017

Variables that strongly modulate the interactions between ΔQ_S and Q^* can be informed by the S results (Figure 4). For instance, a greater range in $K_\downarrow$ (i.e. larger A_K) will occur with larger energy input from solar radiation, leading to stronger heating of the near-surface atmosphere and a smaller portion to ΔQ_S (smaller a_1) but higher baseline ΔQ_S (larger a_3). This is consistent with a reduction in $\overline{K_\downarrow}$ having a decrease in a_3. The temporal change in ΔQ_S is highly correlated with the change in τ, an increase in which implies a slower response of the surface to solar radiation and an overall decrease in ΔQ_S (smaller a_1, a_2 and a_3). The greater sensitivity to τ of a_2 is a key part of the original hysteresis nature of the heating/cooling of a surface. The sensitivity responses of a_1, a_2 and a_3 to U are very consistent with those to C_h, suggesting the similar pathway that turbulent fluxes (i.e. Q_H and Q_E) modulate ΔQ_S. As W mostly influences the heat conduction-diffusion in the underlying surface as thermal properties (i.e. C_p and k), less dependence is observed on it. This is similar with C_p and k.

4 Model Evaluation

In this section, the actual ability of AnOHM to determine the storage heat flux relative to observations is evaluated using 30 min observations from five sites of different land use/covers (Table 3). The measurements include turbulent sensible and latent fluxes, along with incoming and outgoing shortwave and longwave radiation and basic meteorological variables (refer to Kotthaus and Grimmond (2014a; 2014b), Klazura et al. (2006), Coulter et al. (2006), Goulden et al. (2006), Scott et al. (2009), and Luo et al. (2007) for details). Anthropogenic heat flux Q_F at the urban site (i.e., UK-Ldn) is estimated using the GreaterQF model (Iamarino et al., 2011); the heat storage flux ΔQ_S is thus estimated as the modified residual of urban energy balance as $\Delta Q_S = Q^* + 0.75Q_F - 1.2(Q_H + Q_E)$ (Kotthaus and Grimmond, 2014a; 2014b), which is then used in this evaluation. A similar approach for estimating ΔQ_S (i.e., residual of surface energy balance, $\Delta Q_S = Q^* + Q_F - (Q_H + Q_E)$) is applied at other natural sites but with $Q_F = 0$.

AnOHM is first calibrated with observations under sunny conditions, when the assumptions of AnOHM are best satisfied (i.e., diurnal cycles of $K_\downarrow$ and T_a follow sinusoidal forms), to obtain surface properties required by AnOHM (Table 4). As the Bowen ratio β varies daily and monthly (Kotthaus and Grimmond, 2014a; 2014b), β is either determined as the daily value if available, or based on the observation-based monthly climatology (Table 4). The seasonality in albedo α is accounted for also by using its monthly climatology (Table 4). AnOHM is driven by atmospheric forcing (i.e., $K_\downarrow$, T_a, and U) and/or their derived scales (A_K, $\overline{K_\downarrow}$, A_T, $\overline{T_a}$ and τ) to generate the OHM coefficients (i.e., a_1, a_2 and a_3, cf. Figure 5), from which the net heat storage flux ΔQ_S can be predicted (Figure 6) using the observed Q^* with equation 2.

Intra-annual variations are found in all the three OHM coefficients (Figure 5), indicating the strong impact of seasonality of meteorological conditions. These controls, as indicated by eqns 23–25(27), are complex and will vary with local conditions. For instance, comparison of OHM coefficients between the AnOHM predictions (LOESS fitted solid lines in Figure 5; details of LOESS fitting refer to Cleveland and Devlin (1988)) and observations at an asphalt road site in Alland, Austria reported in

Geosci. Model Dev. Discuss., doi:10.5194/gmd-2016-300, 2017
Manuscript under review for journal Geosci. Model Dev.
Published: 10 January 2017

Geoscientific Model Development Discussions

Anandakumar (1999) (empty squares in Figure 5) demonstrates differences in a_1 (Figure 5a) and a_2 (Figure 5b) but general similarity in a_3 (Figure 5c). Compared to a_1 and a_2, it is noteworthy that, in addition to the S results (cf. Figure 4) given the more explicit mechanism by which the atmospheric conditions moderate a_3 (cf. equation 25/27), such seasonality in a_3 is predicted by AnOHM, and evident in the observations (Figure 5c, also Ward et al. (2013)). Larger $\overline{K_\downarrow}$ in warm seasons (May–September) will lead to smaller a_3 (cf. equation 25/27) and *vice versa*. This demonstrates the ability of AnOHM to capture intra-annual dynamics of ΔQ_S.

The simulated and observed ΔQ_S agree well at the five different land cover sites, with RMSE values of ~30 W m^{-2}. For comparison purposes, it is noted that the urban land surface model comparison (Best and Grimmond, 2015; Grimmond et al., 2011), found ΔQ_S to be the most poorly represented among all the SEB components with the best RMSE values of 53 W m^{-2} (Lipson et al., 2016). Although the much smaller ΔQ_S RMSE obtained by AnOHM uses a prescribed Bowen ratio in the offline evaluation, such improvement indicates the ability of AnOHM to simulate a more consistent ΔQ_S with observations. In addition, AnOHM reproduces the seasonality in ΔQ_S well (Figure 6). The negative mean bias error at all five sites indicates ΔQ_S is underestimated by AnOHM. Using a criterion of 50 W m^{-2}, the hit rate percentage (details refer to Schlunzen and Katzfey (2003)) ranges from 60% to 80% for the simulated ΔQ_S. Overall, the evaluation demonstrates good performance of AnOHM in predicting the long-term ΔQ_S with clear seasonality reproduced across a wide range of surface types.

5 Concluding Remarks

In this study, an Analytical Objective Hysteresis Model (AnOHM) is developed to provide a mechanism to obtain OHM coefficients across a wide range of surface and meteorological conditions and to improve physical understanding of the interactions between ΔQ_S and Q^*. The sensitivity of AnOHM to surface properties and hydrometeorological conditions are analysed through Monte Carlo based Subset Simulations (Au and Beck, 2001). The results highlight the importance of the albedo, the Bowen ratio and the bulk transfer coefficient, and the importance of solar radiation and wind speed in regulating the heat storage.

An offline evaluation of AnOHM using flux observations from five sites with different land covers demonstrates its ability to predict the intra-annual dynamics of OHM coefficients and shows good agreement between simulated and observed heat storage fluxes. In particular, the seasonality in the OHM coefficient a_3 observed in a previous study (Anandakumar, 1999) is well predicted by AnOHM. AnOHM will allow improved modelling of the surface energy balance through its physically-based parameterization scheme for storage heat flux ΔQ_S. The overall improvements from adopting AnOHM in modelling land surface processes will be presented in the forthcoming work in the SUEWS-AnOHM framework.

Code availability

The Fortran source code for AnOHM can be obtained from the corresponding authors upon request.

Acknowledgement

Funding is acknowledged from Met Office/Newton Fund CSSP- China (SG), National Science Foundation of China (51679119, TS), and U.S. National Science Foundation (CBET-1435881, ZHW). The authors thank Professor Ivan Au (University of Liverpool) for providing the Subset Simulation package. The authors acknowledge the large number of people who have contributed to the data collection, the agencies that have provided sites and the agencies that have funded the research at the individual sites. The US Department of Energy's Office of Science funded AmeriFlux data (ameriflux-data.lbl.gov) are from: US-Wlr (PIs: Dr David Cook and Dr Richard L. Coulter), CA-NS5 (PI: Dr Mike Goulden), US-SRM (PI: Dr Russell Scott) and US-SO4 (PI: Dr Walt Oechel, funded by San Diego State University and SDSU Field Stations Program). The London data are supported by NERC ClearfLo (NE/H003231/1), NERC/Belmont TRUC (NE/L008971/1), EUf7 BRIDGE (211345), H2020 UrbanFluxes (637519), King's College London and University of Reading. In particular, the authors thank Dr Simone Kotthaus (University of Reading) for the UK-Ldn site data. For access to the UK-Ldn site data, please contact c.s.grimmond@reading.ac.uk.

References:

Allen, L., Lindberg, F. and Grimmond, C. S. B.: Global to city scale urban anthropogenic heat flux: model and variability, Int. J. Climatol., 31(13), 1990–2005, doi:10.1002/joc.2210, 2011.

Anandakumar, K.: A study on the partition of net radiation into heat fluxes on a dry asphalt surface, Atmos. Environ., 33(24–25), 3911–3918, doi:10.1016/S1352-2310(99)00133-8, 1999.

Ao, X., Grimmond, C. S. B., Chang, Y., Liu, D., Tang, Y., Hu, P., Wang, Y., ZOU, J. and Tan, J.: Heat, water and carbon exchanges in the tall megacity of Shanghai: challenges and results, Int. J. Climatol., n/a–n/a, doi:10.1002/joc.4657, 2016.

Arnfield, A. J. and Grimmond, C. S. B.: An urban canyon energy budget model and its application to urban storage heat flux modeling, Energ. Buildings, 27(1), 61–68, doi:10.1016/S0378-7788(97)00026-1, 1998.

Au, S. K. and Beck, J. L.: Subset simulation and its application to seismic risk based on dynamic analysis, Journal of Engineering Mechanics-Asce, 129(8), 901–917, doi:10.1061/(ASCE)0733-9399(2003)129:8(901), 2003.

Au, S. K. and Beck, J. L.: Estimation of small failure probabilities in high dimensions by subset simulation, Probabilistic Engineering Mechanics, 16(4), 263–277, doi:10.1016/S0266-8920(01)00019-4, 2001.

Au, S. K., Ching, J. and Beck, J. L.: Application of subset simulation methods to reliability benchmark problems, Structural Safety, 29(3), 183–193, doi:10.1016/j.strusafe.2006.07.008, 2007.

Best, M. J. and Grimmond, C. S. B.: Key Conclusions of the First International Urban Land Surface Model Comparison Project, Bull. Amer. Meteor. Soc., 96(5), 805–819, doi:10.1175/BAMS-D-14-00122.1, 2015.

Best, M. J. and Grimmond, C. S. B.: Investigation of the impact of anthropogenic heat flux within an urban land surface model and PILPS-urban, Theor. Appl. Climatol., 126(1), 51–60, doi:10.1007/s00704-015-1554-3, 2016.

Camuffo, D. and Bernardi, A.: An observational study of heat fluxes and their relationships with net radiation, Boundary-Layer Meteorol., 23(3), 359–368, doi:10.1007/BF00121121, 1982.

Chen, F. and Dudhia, J.: Coupling an advanced land surface-hydrology model with the Penn State-NCAR MM5 modeling system. Part I: Model implementation and sensitivity, Mon. Weather Rev., 129(4), 569–585, doi:10.1175/1520-0493(2001)129<0569:CAALSH>2.0.CO;2, 2001.

Ching, J. K. S., Clarke, J. F. and Godowitch, J. M.: Modulation of heat flux by different scales of advection in an urban environment, Boundary-Layer Meteorol., 25(2), 171–191, doi:10.1007/BF00123973, 1983.

Chow, W. T. L., Salamanca, F. P., Georgescu, M., Mahalov, A., Milne, J. M. and Ruddell, B. L.: A multi-method and multi-scale approach for estimating city-wide anthropogenic heat fluxes, Atmos. Environ., 99, 64–76, doi:10.1016/j.atmosenv.2014.09.053, 2014.

Cleveland, W. S. and Devlin, S. J.: Locally Weighted Regression: An Approach to Regression Analysis by Local Fitting, Journal of the American Statistical Association, 83(403), 596–610, doi:10.1080/01621459.1988.10478639, 1988.

Coulter, R. L., Pekour, M. S., Cook, D. R., Klazura, G. E., Martin, T. J. and Lucas, J. D.: Surface energy and carbon dioxide fluxes above different vegetation types within ABLE, Agr. Forest. Meteorol., 136(3-4), 147–158, doi:10.1016/j.agrformet.2004.11.011, 2006.

Doll, D., Ching, J. and Kaneshiro, J.: Parameterization of subsurface heating for soil and concrete using net radiation data, Boundary-Layer Meteorol., 32(4), 351–372, doi:10.1007/BF00122000, 1985.

Gao, Z., Fan, X. G. and Bian, L. G.: An analytical solution to one-dimensional thermal conduction-convection in soil, Soil Science, 168(2), 99–107, doi:10.1097/01.ss.0000055305.23789.be, 2003.

Gao, Z., Horton, R. and Liu, H. P.: Impact of wave phase difference between soil surface heat flux and soil surface temperature on soil surface energy balance closure, J. Geophys. Res., 115(D16), D16112, doi:10.1029/2009JD013278, 2010.

Gao, Z., Lenschow, D. H., Horton, R., Zhou, M., Wang, L. and Wen, J.: Comparison of two soil temperature algorithms for a bare ground site on the Loess Plateau in China, J Geophys Res-Oc Atm, 113(D18), D18105, 2008.

Goulden, M. L., Winston, G. C., McMillan, A. M. S., Litvak, M. E., Read, E. L., Rocha, A. V. and Elliot, J. R.: An eddy covariance mesonet to measure the effect of forest age on land-atmosphere exchange, Glob Change Biol, 12(11), 2146–2162, doi:10.1111/j.1365-2486.2006.01251.x, 2006.

Grimmond, C. S. B. and Oke, T. R.: Heat storage in urban areas: local-scale observations and evaluation of a simple model, J Appl Meteorol, 38(7), 922–940, doi:10.1175/1520-0450(1999)038<0922:HSIUAL>2.0.CO;2, 1999.

Grimmond, C. S. B. and Oke, T. R.: Turbulent heat fluxes in urban areas: Observations and a local-scale urban meteorological parameterization scheme (LUMPS), J Appl Meteorol, 41(7), 792–810, 2002.

Grimmond, C. S. B., Blackett, M., Best, M. J., Baik, J. J., Belcher, S. E., Beringer, J., Bohnenstengel, S. I., Calmet, I., Chen, F., Coutts, A., Dandou, A., Fortuniak, K., Gouvea, M. L., Hamdi, R., Hendry, M., Kanda, M., Kawai, T., Kawamoto, Y., Kondo, H., Krayenhoff, E. S., Lee, S.-H., Loridan, T., Martilli, A., Masson, V., Miao, S., Oleson, K., Ooka, R., Pigeon, G., Porson, A., Ryu, Y.-H., Salamanca, F. P., Steeneveld, G. J., Tombrou, M., Voogt, J. A., Young, D. T. and Zhang, N.: Initial results from Phase 2 of the international urban energy balance model comparison, Int. J. Climatol., 31(2), 244–272, doi:10.1002/joc.2227, 2011.

Grimmond, C. S. B., Cleugh, H. A. and Oke, T. R.: An objective urban heat storage model and its comparison with other schemes, Atmos. Environ. B-Urb, 25(3), 311–326, doi:10.1016/0957-1272(91)90003-W, 1991.

Hastings, W. K.: Monte carlo sampling methods using Markov chains and their applications, Biometrika, 57(1), 97–109, doi:10.1093/biomet/57.1.97, 1970.

Iamarino, M., Beevers, S. and Grimmond, C. S. B.: High-resolution (space, time) anthropogenic heat emissions: London 1970-2025, Int. J. Climatol., 32(11), 1754–1767, doi:10.1002/joc.2390, 2011.

Järvi, L., Grimmond, C. S. B. and Christen, A.: The Surface Urban Energy and Water Balance Scheme (SUEWS): Evaluation in Los Angeles and Vancouver, J Hydrol, 411(3-4), 219–237, doi:10.1016/j.jhydrol.2011.10.001, 2011.

Järvi, L., Grimmond, C. S. B., Taka, M., Nordbo, A., Setälä, H. and Strachan, I. B.: Development of the Surface Urban Energy and Water Balance Scheme (SUEWS) for cold climate cities, Geoscientific Model Development, 7(4), 1691–1711, doi:10.5194/gmd-7-1691-2014, 2014.

Karsisto, P., Fortelius, C., Demuzere, M., Grimmond, C. S. B., Oleson, K. W., Kouznetsov, R., Masson, V. and Järvi, L.: Seasonal surface urban energy balance and wintertime stability simulated using three land-surface models in the high-latitude city Helsinki, Q.J.R. Meteorol. Soc., 142(694), 401–417, doi:10.1002/qj.2659, 2015.

Katul, G. G., Oren, R., Manzoni, S., Higgins, C. W. and Parlange, M. B.: Evapotranspiration: a process driving mass transport and energy exchange in the soil-plant-atmosphere-climate system, Rev. Geophys., 50(3), RG3002, doi:10.1029/2011RG000366, 2012.

Kerschgens, M. J. and Drauschke, R. L.: On the energy budget of a wintry mid-latitude city atmosphere, Beiträge zur Physik der Atmosphäre, 59(1), 115–125, 1986.

Kerschgens, M. J. and Hacker, J. M.: On the energy budget of the convective boundary layer over an urban and rural environment, Beiträge zur Physik der Atmosphäre, 58(2), 171–185, 1985.

Kerschgens, M. J. and Kraus, H.: On the energetics of the urban canopy layer, Atmos. Environ. B-Urb, 24(2), 321–328, doi:10.1016/0957-1272(90)90038-V, 1990.

Klazura, G. E., Cook, D. R., Coulter, R. L., Hart, R. L., Holdridge, D. J., Lesht, B. M., Lucas, J. D., Martin, T. J., Pekour, M. S. and Wesely, M. L.: Atmospheric boundary layer measurements in south-central Kansas, 1997-2004, Bull. Amer. Meteor. Soc., 87(10), 1319–1324, doi:10.1175/BAMS-87-10-1319, 2006.

Kotthaus, S. and Grimmond, C. S. B.: Energy exchange in a dense urban environment – Part I: Temporal variability of long-term observations in central London, Urban Climate, 10, 261–280, doi:10.1016/j.uclim.2013.10.002, 2014a.

Kotthaus, S. and Grimmond, C. S. B.: Energy exchange in a dense urban environment – Part II: Impact of spatial heterogeneity of the surface, Urban Climate, 10, 281–307, doi:10.1016/j.uclim.2013.10.001, 2014b.

Kotthaus, S., Smith, T. E. L., Wooster, M. J. and Grimmond, C. S. B.: Derivation of an urban materials spectral library through emittance and reflectance spectroscopy, ISPRS Journal of Photogrammetry and Remote Sensing, 94, 194–212, doi:10.1016/j.isprsjprs.2014.05.005, 2014.

Li, D., Sun, T., Liu, M., Yang, L., Wang, L. and Gao, Z.: Contrasting responses of urban and rural surface energy budgets to heat waves explain synergies between urban heat islands and heat waves, Environ Res Lett, 10(5), 054009, doi:10.1088/1748-9326/10/5/054009, 2015.

Liang, X., Lettenmaier, D. P., Wood, E. F. and Burges, S. J.: A simple hydrologically based model of land surface water and energy fluxes for general circulation models, J. Geophys. Res., 99(D7), 14415–14428, doi:10.1029/94JD00483, 1994.

Lipson, M. J., Hart, M. A. and Thatcher, M.: Efficiently modelling urban heat storage: an interface conduction scheme in the aTEB urban land surface model, Geoscientific Model Development, 1–28, doi:10.5194/gmd-2016-240, 2016.

Luo, H., Oechel, W. C., Hastings, S. J., Zulueta, R., Qian, Y. and Kwon, H.: Mature semiarid chaparral ecosystems can be a significant sink for atmospheric carbon dioxide, Glob Change Biol, 13(2), 386–396, doi:10.1111/j.1365-2486.2006.01299.x, 2007.

Masson, V., Grimmond, C. S. B. and Oke, T. R.: Evaluation of the Town Energy Balance (TEB) scheme with direct measurements from dry districts in two cities, J Appl Meteorol, 41(10), 1011–1026, 2002.

McCumber, M. C. and Pielke, R. A.: Simulation of the effects of surface fluxes of heat and moisture in a mesoscale numerical model: 1. Soil layer, J Geophys Res-Oc Atm, 86(C10), 9929–9938, doi:10.1029/JC086iC10p09929, 1981.

Metropolis, N., Rosenbluth, A. W., Rosenbluth, M. N., Teller, A. H. and Teller, E.: Equation of State Calculations by Fast Computing Machines, The Journal of Chemical Physics, 21(6), 1087–1092, doi:10.1063/1.1699114, 1953.

Meyn, S. K. and Oke, T. R.: Heat fluxes through roofs and their relevance to estimates of urban heat storage, Energ. Buildings, 41(7), 745–752, doi:10.1016/j.enbuild.2009.02.005, 2009.

Nie, W.-S., Sun, T. and Ni, G.-H.: Spatiotemporal characteristics of anthropogenic heat in an urban environment: A case study of Tsinghua Campus, Build. Environ., 82, 675–686, doi:10.1016/j.buildenv.2014.10.011, 2014.

Offerle, B. D., Grimmond, C. S. B. and Fortuniak, K.: Heat storage and anthropogenic heat flux in relation to the energy balance of a central European city centre, Int. J. Climatol., 25(10), 1405–1419, doi:10.1002/joc.1198, 2005.

Oke, T. R.: The urban energy balance, Progress in Physical Geography, 12(4), 471–508, doi:10.1177/030913338801200401, 1988.

Oke, T. R. and Cleugh, H. A.: Urban heat storage derived as energy balance residuals, Boundary-Layer Meteorol., 39(3), 233–245, doi:10.1007/BF00116120, 1987.

Oke, T. R., Kalanda, B. D. and Steyn, D. G.: Parameterization of heat storage in urban areas, Urban Ecology, 5(1), 45–54, doi:10.1016/0304-4009(81)90020-6, 1981.

Oliphant, A. J., Grimmond, C. S. B., Zutter, H. N., Schmid, H. P., Su, H. B., Scott, S. L., Offerle, B. D., Randolph, J. C. and Ehman, J.: Heat storage and energy balance fluxes for a temperate deciduous forest, Agr. Forest. Meteorol., 126(3-4), 185–201, doi:10.1016/j.agrformet.2004.07.003, 2004.

Pauwels, V. R. N. and Daly, E.: Advantages of analytically computing the ground heat flux in land surface models, Hydrol. Earth Syst. Sci., 20(11), 4689–4706, doi:10.5194/hess-20-4689-2016, 2016.

Ren, T., Kluitenberg, G. J. and Horton, R.: Determining Soil Water Flux and Pore Water Velocity by a Heat Pulse Technique, Soil Sci. Soc. Am. J., 64(2), 552, doi:10.2136/sssaj2000.642552x, 2000.

Roberts, S. M., Oke, T. R., Grimmond, C. S. B. and Voogt, J. A.: Comparison of Four Methods to Estimate Urban Heat Storage, J Appl Meteorol Clim, 45(12), 1766–1781, doi:10.1175/JAM2432.1, 2006.

Roberts, S. M., Oke, T. R., Grimmond, C. S. B. and Voogt, J. A.: Comparison of Four Methods to Estimate Urban Heat Storage,, 45(12), 1766–1781, doi:10.1175/JAM2432.1, 2009.

Roth, M. and Oke, T. R.: Relative Efficiencies of Turbulent Transfer of Heat, Mass, and Momentum over a Patchy Urban Surface, J. Atmos. Sci., 52(11), 1863–1874, doi:10.1175/1520-0469(1995)052<1863:reotto>2.0.co;2, 1995.

Sailor, D. J.: A review of methods for estimating anthropogenic heat and moisture emissions in the urban environment, edited by M. Roth, R. Emmanuel, T. Ichinose, and J. Salmond, Int. J. Climatol., 31(2), 189–199, doi:10.1002/joc.2106, 2011.

Schlunzen, K. H. and Katzfey, J. J.: Relevance of sub-grid-scale land-use effects for mesoscale models, Tellus A, 55(3), 232–246, doi:10.1034/j.1600-0870.2003.00017.x, 2003.

Scott, R. L., Jenerette, G. D., Potts, D. L. and Huxman, T. E.: Effects of seasonal drought on net carbon dioxide exchange from a woody-plant-encroached semiarid grassland, J. Geophys. Res. Biogeosci., 114(G4), doi:10.1029/2008JG000900, 2009.

Sellers, P. J., DICKINSON, R. E., Randall, D. A., Betts, A. K., Hall, F. G., Berry, J. A., Collatz, G. J., Denning, A. S., Mooney, H. A., Nobre, C. A., Sato, N., Field, C. B. and Henderson-Sellers, A.: Modeling the Exchanges of Energy, Water, and Carbon Between Continents and the Atmosphere, Science, 275(5299), 502–509, doi:10.1126/science.275.5299.502, 1997.

Souch, C., Grimmond, C. S. B. and Wolfe, C. P.: Evapotranspiration rates from wetlands with different disturbance histories: Indiana Dunes National Lakeshore, Wetlands, 18(2), 216–229, doi:10.1007/BF03161657, 1998.

Staley, D. O. and Jurica, G. M.: Effective Atmospheric Emissivity under Clear Skies, J Appl Meteorol, 11(2), 349–356, doi:10.1175/1520-0450(1972)011<0349:eaeucs>2.0.co;2, 1972.

Stull, R.: An Introduction to boundary layer meteorology, Springer. 1988.

Sun, T., Wang, Z.-H. and Ni, G.-H.: Revisiting the hysteresis effect in surface energy budgets, Geophys. Res. Lett., 40(9), 1741–1747, doi:10.1002/grl.50385, 2013.

Wang, Z.-H.: Reconstruction of soil thermal field from a single depth measurement, J Hydrol, 464–465(0), 541–549, doi:10.1016/j.jhydrol.2012.07.047, 2012.

Wang, Z.-H., Bou-Zeid, E. and Smith, J. A.: A coupled energy transport and hydrological model for urban canopies evaluated using a wireless sensor network, Q.J.R. Meteorol. Soc., 139(675), 1643–1657, doi:10.1002/qj.2032, 2012.

Geosci. Model Dev. Discuss., doi:10.5194/gmd-2016-300, 2017
Manuscript under review for journal Geosci. Model Dev.
Published: 10 January 2017

Wang, Z.-H., Bou-Zeid, E., Au, S. K. and Smith, J. A.: Analyzing the Sensitivity of WRF's Single-Layer Urban Canopy Model to Parameter Uncertainty Using Advanced Monte Carlo Simulation, J Appl Meteorol Clim, 50(9), 1795–1814, doi:10.1175/2011JAMC2685.1, 2011.

Ward, H. C., Evans, J. G. and Grimmond, C. S. B.: Multi-season eddy covariance observations of energy, water and carbon fluxes over a suburban area in Swindon, UK, Atmos. Chem. Phys., 13(9), 4645–4666, doi:10.5194/acp-13-4645-2013, 2013.

Ward, H. C., Kotthaus, S., Järvi, L. and Grimmond, C. S. B.: Surface Urban Energy and Water Balance Scheme (SUEWS): Development and evaluation at two UK sites, Urban Climate, doi:10.1016/j.uclim.2016.05.001, 2016.

Yang, J. and Wang, Z.-H.: Land surface energy partitioning revisited: A novel approach based on single depth soil measurement, Geophys. Res. Lett., 41(23), 8348–8358, doi:10.1002/2014GL062041, 2014.

Yang, J., Wang, Z.-H., Chen, F., Miao, S., Tewari, M., Voogt, J. A. and Myint, S.: Enhancing Hydrologic Modelling in the Coupled Weather Research and Forecasting–Urban Modelling System, Boundary-Layer Meteorol., 155(1), 1–23, doi:10.1007/s10546-014-9991-6, 2014.

Geosci. Model Dev. Discuss., doi:10.5194/gmd-2016-300, 2017
Manuscript under review for journal Geosci. Model Dev.
Published: 10 January 2017

Geoscientific Model Development Discussions
Open Access

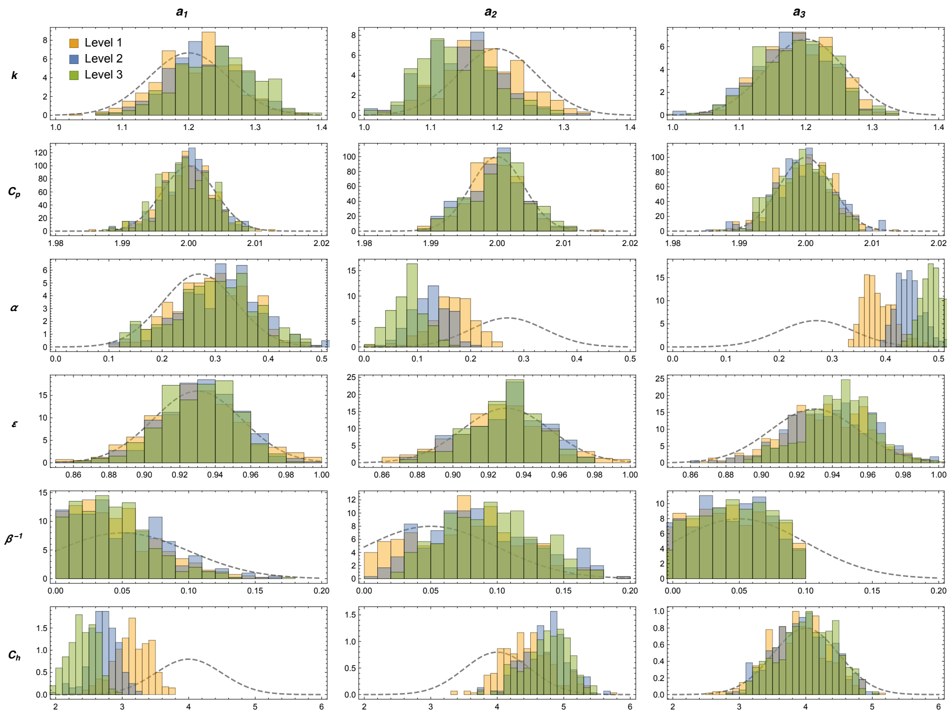

Figure 1 Histograms of conditional samples at different conditional levels for surface property parameters (shown in rows from top to bottom for thermal conductivity k in W m^{-1} K^{-1}, heat capacity C_p in MJ m^{-3} K^{-1}, albedo α, emissivity ε, inverse Bowen ratio β^{-1} and bulk transfer coefficient C_h in J m^{-3} K^{-1}, respectively) with AnOHM coefficients as the model output (shown in columns from left to right for a_1, a_2 and a_3, respectively). In each subplot, the x-axis indicates the parameter value while the y-axis shows the PDF value; the dashed line denotes the original proposal distribution. Simulation levels are shown in different colors.

Geosci. Model Dev. Discuss., doi:10.5194/gmd-2016-300, 2017
Manuscript under review for journal Geosci. Model Dev.
Published: 10 January 2017

Geoscientific Model Development Discussions
Open Access

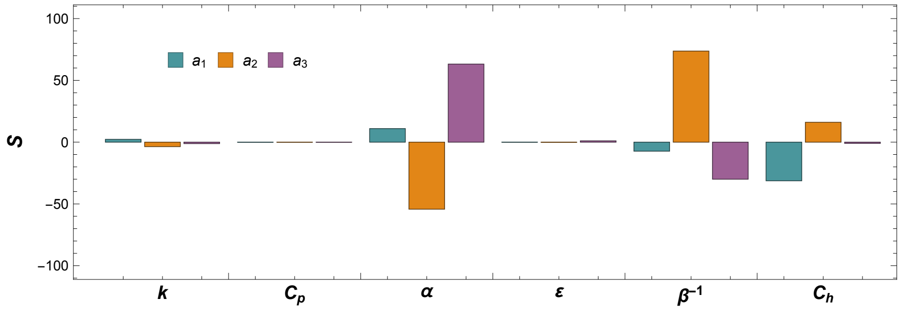

Figure 2 Relative variation in sensitivity (S, %, equation 28) to surface parameters. See Figure 1 for further details.

Geosci. Model Dev. Discuss., doi:10.5194/gmd-2016-300, 2017
Manuscript under review for journal Geosci. Model Dev.
Published: 10 January 2017

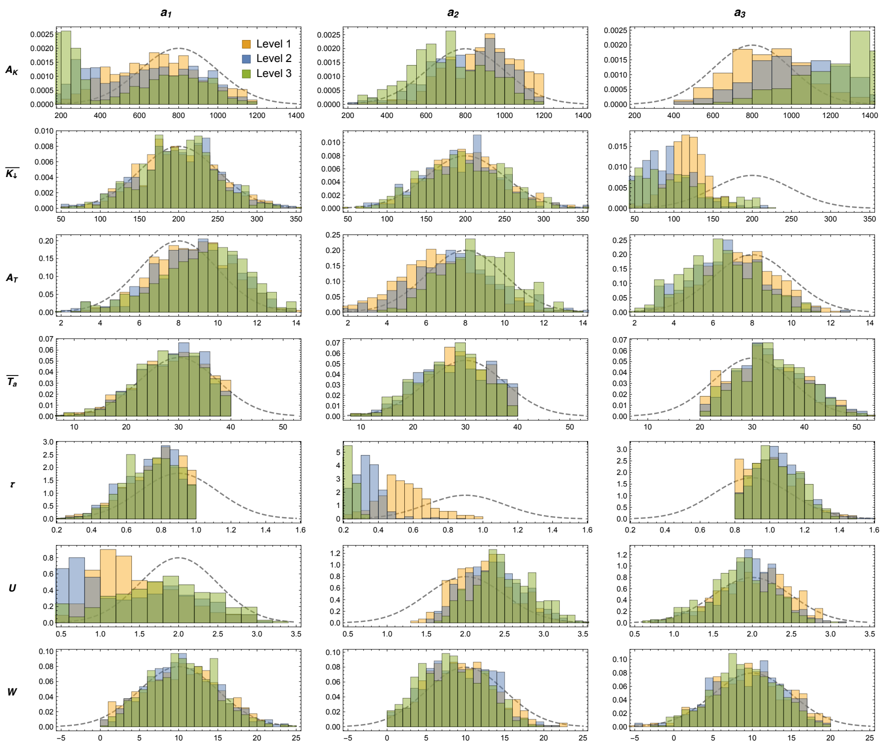

Figure 3 Histograms of conditional samples at different conditional levels for ambient forcing parameters (shown in rows from top to bottom for incoming solar radiation amplitude A_K in W m^{-2} and its daytime mean $\overline{K_\downarrow}$ in W m^{-2}, air temperature amplitude A_T in °C and its daily mean $\overline{T_a}$ in °C, the phase lag τ in rad between $K_\downarrow$ and T_a, wind speed U in m s^{-1} and water flux density W in m s^{-1}, respectively) with AnOHM coefficients as the model output (shown in columns from left to right for a_1, a_2 and a_3, respectively). In each subplot, the x-axis indicates the parameter value while the y-axis shows the PDF value; the dashed line denotes the original proposal distribution. Simulation levels are shown in different colors.

Geosci. Model Dev. Discuss., doi:10.5194/gmd-2016-300, 2017
Manuscript under review for journal Geosci. Model Dev.
Published: 10 January 2017

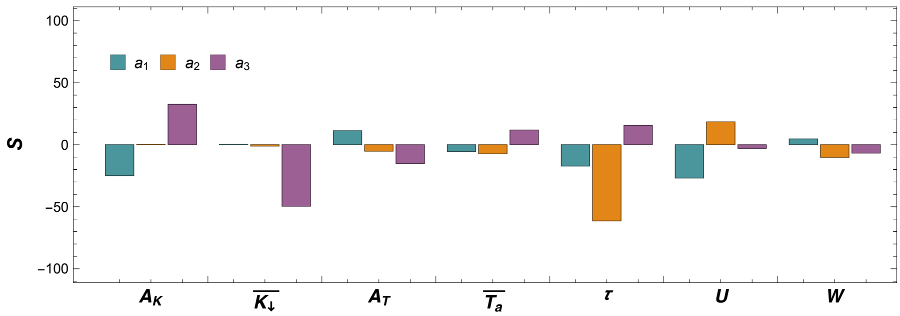

Figure 4 Relative variation in sensitivity (*S*, %, equation 28) to forcing parameters. See Figure 3 for further details.

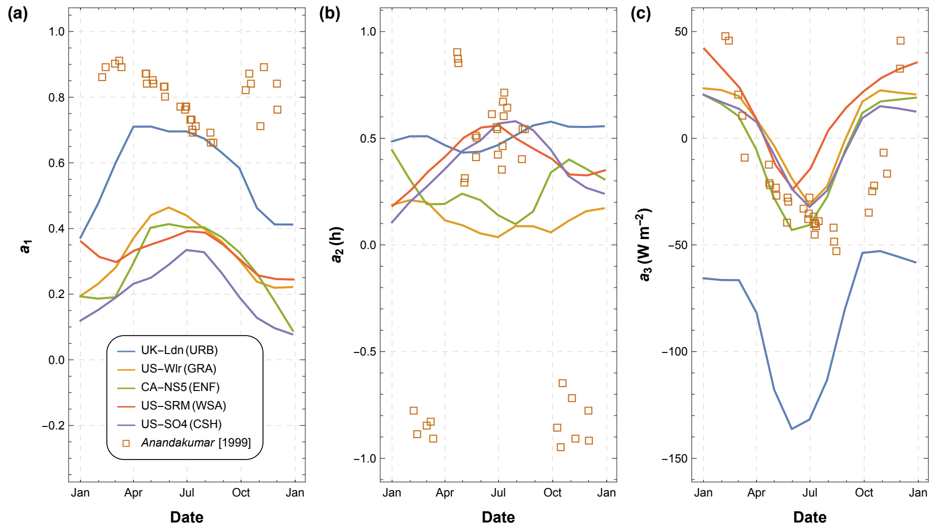

Figure 5 Intra-annual variations of OHM coefficients: (a) a_1, (b) a_2 and (c) a_3. The solid lines denote LOESS fits of daily values predicted by AnOHM. The squares show daily values measured at an asphalt road site in Anandakumar (1999). The LOESS fitting is a local polynomial regression approach, whose details refer to Cleveland and Devlin (2012).

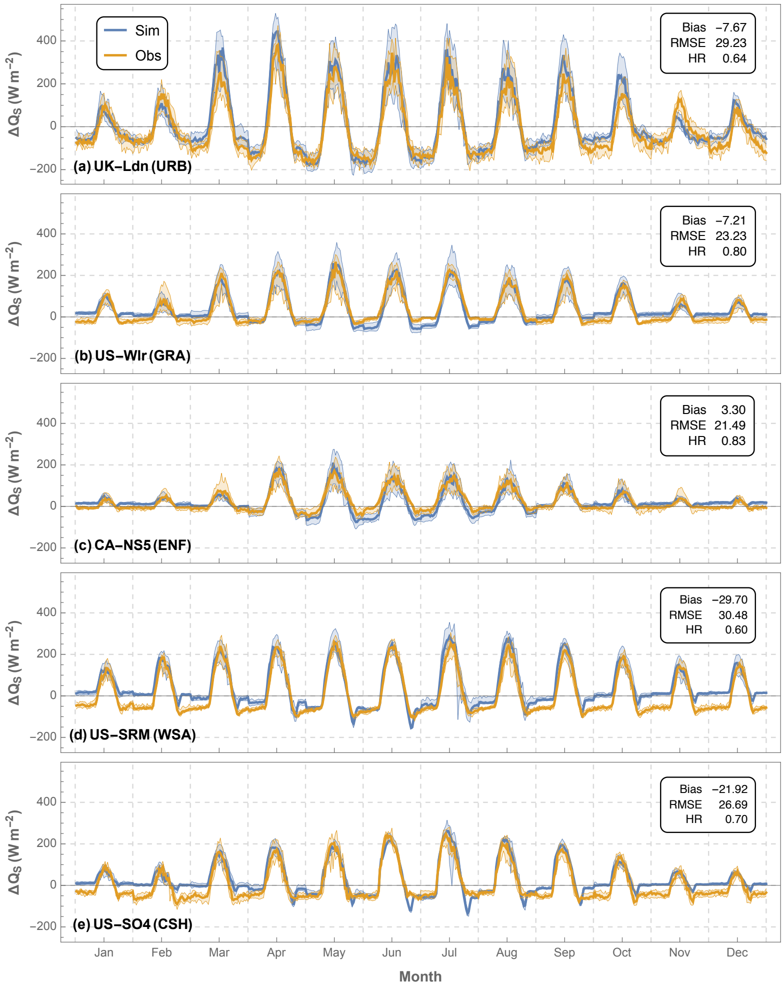

Figure 6 The monthly median (line) diurnal cycles and interquartile (shaded) values of ΔQ_S for AnOHM predictions (blue) and observations (orange) at (a) UK-Ldn (URB), (b) US-Wlr (GRA), (c) CA-NS5 (ENF), (d) US-SRM (WSA), and (e) US-SO4 (CSH) (see Table 2 for site information). Statistics include average bias, RMSE, and hit rate ((Schlunzen and Katzfey, 2003), criteria is 50 W m^{-2}).

Geosci. Model Dev. Discuss., doi:10.5194/gmd-2016-300, 2017
Manuscript under review for journal Geosci. Model Dev.
Published: 10 January 2017

Geoscientific Model Development Discussions
Open Access
EGU

Table 1 Range of values used as basis for the sensitivity analysis (a) surface parameters and (b) meteorological variables. All are assumed to have normal PDF. Values of surface parameters are based on values reported in Stull (1982).

Parameter/Variable		Unit	Min	Max	Mean	Standard deviation
(a) Surface						
thermal conductivity	k	W m^{-1} K^{-1}	0	3	1.2	0.1
bulk material heat capacity	C_p	MJ m^{-3} K^{-1}	0	4	2.0	0.04
albedo	α	--	0	1	0.27	0.07
emissivity	ε	--	0.8	1.0	0.93	0.025
midday* mean Bowen ratio (inverse)	β^{-1}	--	0	20	0.05	0.05
bulk transfer coefficient	C_h	J m^{-3} K^{-1}	0	8	4	0.5
(b) Hydrometeorological						
Amplitude or range of the daily incoming shortwave radiation	A_K	W m^{-2}	0	1200	800	200
Mean daytime incoming shortwave radiation	$\overline{K_\downarrow}$	W m^{-2}	0	500	200	50
Amplitude or range of the daily air temperature	A_T	ºC	0	15	8	2
Mean daily air temperature	$\overline{T_a}$	ºC	0	40	30	7.5
Phase lag between radiation and air temperature	τ	rad	0	$\pi/2$	$\pi/4$	$\pi/10$
Mean daytime wind speed	U	m s^{-1}	0	4	2	0.5
Mean daily water flux density	W	10^{-7} m^{3} s^{-1} m^{-2}	0	100	10	5

* midday period: 1000–1400 local standard time.

Table 2 Characteristics of the flux towers at the study sites.

Site	UK-Ldn	US-Wlr	CA-NS5	US-SRM	US-SO4
Location	51.50º N 0.12º W	37.52º N 96.86º W	55.86º N 98.49º W	31.82º N 110.87º W	33.38º N 116.64º W
Land cover classification	Urban/ Built-up	Grassland	Evergreen Needleleaf Forest	Woody Savannas	Closed Shrublands
Land cover code	URB	GRA	ENF	WSA	CSH
Study Year	2011	2003	2004	2004	2005
Reference	Kotthaus and Grimmond (2014a; 2014b)	Klazura et al. (2006), Coulter et al. (2006)	Goulden et al. (2006)	Scott et al. (2009)	Luo et al. (2007)

Geosci. Model Dev. Discuss., doi:10.5194/gmd-2016-300, 2017
Manuscript under review for journal Geosci. Model Dev.
Published: 10 January 2017

Geoscientific Model Development Discussions Open Access EGU

Table 3 Surface properties used in AnOHM simulation for the study sites based on calibration. The values of α and β are monthly climatology from January to December and are used when observations are not available (see Table 1 for notation definition).

Parameter	Unit	Site				
		UK-Ldn	US-Wlr	CA-NS5	US-SRM	US-SO4
k	W m^{-1} K^{-1}	2.8	0.43	0.51	0.41	0.56
C_p	MJ m^{-3} K^{-1}	2.4	0.31	0.36	0.56	0.27
α	--	0.24,0.24, 0.22,0.20, 0.14,0.13, 0.12,0.14, 0.18,0.24, 0.24,0.18	0.29,0.29, 0.17,0.18, 0.18,0.12, 0.11,0.10, 0.19,0.13, 0.24,0.35	0.30,0.29, 0.22,0.15, 0.10,0.10, 0.10,0.11, 0.22,0.24, 0.28,0.30	0.13,0.17, 0.16,0.14, 0.13,0.12, 0.13,0.15, 0.14,0.19, 0.13,0.18	0.22,0.11, 0.11,0.10, 0.11,0.10, 0.10,0.10, 0.11,0.10, 0.17,0.24
ε	--	0.92	0.93	0.95	0.95	0.92
β	--	6.1, 5.1, 8.3, 7.9, 5.4, 3.9, 5.3, 4.2, 5.2, 4.3, 4.8, 3.2	2.9, 0.8, 7.6, 2.7, 0.3, 0.3, 0.3, 0.8, 0.5, 0.7, 2.3, 2.3	6.1, 6.0, 8.7, 8.0, 1.9, 1.6, 0.7, 0.7, 1.3, 1.4, 3.1, 8.0	1.9, 5.5, 3.3, 2.0, 10.1, 9.7, 2.0, 0.9, 3.0, 4.3, 10.0, 3.3	1.5, 1.4, 1.9, 3.0, 1.4, 1.4, 2.1, 1.2, 2.8, 1.9, 2.1, 4.1
C_h	J m^{-3} K^{-1}	4.3	1.9	5.1	3.6	3.9